Environmental Science & Technology

Article

pubs.acs.org/est

Exogenous Electron Shuttle-Mediated Extracellular Electron Transfer of *Shewanella putrefaciens* 200: Electrochemical Parameters and Thermodynamics

Yundang Wu,[†,‡,§] Tongxu Liu,*[,†] Xiaomin Li,[†] and Fangbai Li*[,†]

[†]Guangdong Key Laboratory of Agricultural Environment Pollution Integrated Control, Guangdong Institute of Eco-Environmental and Soil Sciences, Guangzhou, P. R. China

[‡]Guangzhou Institute of Geochemistry, Chinese Academy of Sciences, Guangzhou 510640, P. R. China

[§]University of Chinese Academy of Sciences, Beijing 100039, P. R. China

Supporting Information

ABSTRACT: Despite the importance of exogenous electron shuttles (ESs) in extracellular electron transfer (EET), a lack of understanding of the key properties of ESs is a concern given their different influences on EET processes. Here, the ES-mediated EET capacity of *Shewanella putrefaciens* 200 (SP200) was evaluated by examining the electricity generated in a microbial fuel cell. The results indicated that all the ESs substantially accelerated the current generation compared to only SP200. The current and polarization parameters were linearly correlated with both the standard redox potential (E^0_{ES}) and the electron accepting capacity (EAC) of the ESs. A thermodynamic analysis of the electron transfer from the electron donor to the electrode suggested that the EET from *c*-type cytochromes (*c*-Cyts) to ESs is a crucial step causing the differences in EET capacities among various ESs. Based on the derived equations, both E^0_{ES} and EAC can quantitatively determine potential losses (ΔE) that reflect the potential loss of the ES-mediated EET. In situ spectral kinetic analysis of ES reduction by *c*-Cyts in a living SP200 suspension was first investigated with the E_{ES}, $E_{c\text{-Cyt}}$, and ΔE values being calculated. This study can provide a comprehensive understanding of the role of ESs in EET.

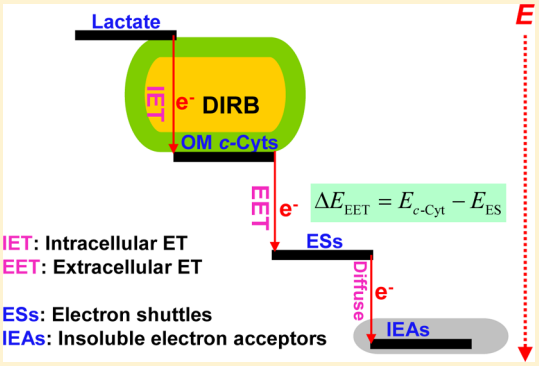

INTRODUCTION

Dissimilatory metal-reducing bacteria can convert biochemical energy for metabolism through extracellular electron transfer (EET), which has been widely reported in both natural systems and artificial devices (e.g., microbial fuel cells).[1−3] Although the direct electron transfer from bacteria to substrates via outer-membrane cytochromes is considered to be the basic EET pathway, the electron shuttles (ESs) play a key role in facilitating the long-range electron transfer from the bacterial cell surface to insoluble electron acceptors (e.g., iron(III) oxides and electrodes) via the cycling of their reduced and oxidized states.[4−10] ESs not only widely exist in aquatic and terrestrial environments (exogenous ESs), but can also be secreted by various microorganism (endogenous ESs).[11−13] The ubiquitousness of ESs and their particular redox properties highlight their environmental significance and their roles in elemental biogeochemistry, contaminant degradation, and some engineering aspects (microbial fuel cells (MFCs), bioremediation, etc.);[14−18] however, the redox behavior of ESs has been poorly characterized, and a fundamental understanding of their redox properties is needed.

The redox potential (E_h), which is an important parameter reflecting the redox properties of ESs, has typically been investigated with respect to its effects on the EET capacities (such as metal reduction and current generation).[19,20] The optimal enhancement of ferric reduction by *Geobacter metallireducens* was observed when their standard redox potentials (E^0_h) fell within a narrow range (−225 to −137 mV),[21] and similar behavior has been observed for other bacteria, including *Klebsiella pneumonia* L17,[20] *Shewanella decolorationis* S12, and *Aeromonas hydrophila* HS01.[22] Hence, no linear correlation between the E^0_h of ESs and iron reduction rates was observed. However, the iron reduction rates exhibited by *Shewanella putrefaciens* CN32 were negatively correlated with the E^0_h of various ESs (−247 mV to 11 mV).[23] The key components in the electron-transfer chain are outer-membrane *c*-type cytochromes (OM *c*-Cyts, such as OmcA, OmcB, MtrC, and OmcS), which have a broad potential windows that span from −320 mV to −15 mV.[24,25] Only the *c*-Cyts with E_h value lower than that of the ES can reduce the ES. The $E_h{}^0$ of the ESs used by O'Loughlin[23] were all higher than −247 mV, suggesting that the *c*-Cyts can reduce all the ESs, while the $E_h{}^0$ of the ESs used by Wolf et al.[21] were just higher than −500

Received: April 8, 2014
Revised: June 8, 2014
Accepted: July 24, 2014
Published: July 24, 2014

dx.doi.org/10.1021/es5017312 | Environ. Sci. Technol. 2014, 48, 9306−9314

mV, indicating that even the *c*-Cyts with the lowest E_h^0 (−320 mV) are not able to reduce the ESs with E_h^0 between −500 mV and −320 mV. While this may be the case, the investigation of the correlation between E_h^0 and electricity generation in the presence of various ESs has rarely been reported.[20,21]

Recently, the electron transfer capacity of ESs has been investigated using electrochemical methods, which is reportedly a promising approach to the direct quantification of the electron transfer capacity during the shutting process of ESs.[26−28] Using this method, researchers investigated the effects of various quinones on the iron reduction rates and electricity generation and observed that the iron reduction rates and amount of current generated were positively and linearly correlated with the electron transfer capacity of quinones.[20,22] The quantitative property−activity relationships among electron transfer capacity, the redox equilibria of quinones (speciation of quinones), and iron reduction rates were established; the electron transfer capacity was observed to be expressed by concentrations of various quinone species and E_h^0, which can be used to predict the properties (both kinetic and thermodynamic aspects) of other ESs or the redox states of ESs under different conditions.[22] However, given the complexity of the ES-mediated EET mechanism, detailed mechanistic studies related to the molecular-level processes that control the relative importance of these EET mechanisms are still needed. Hence, the investigation of the thermodynamics of each elementary reaction in the EET process is important for elucidating the roles of ESs and the critical reaction steps that control the ES-mediated EET processes.

The elementary reaction between OM *c*-Cyts and electron acceptors is widely recognized as being an important step during the EET processes; consequently, some studies have focused on the reduction of metals by the purified OM *c*-Cyts from dissimilatory metal-reducing bacteria.[29−31] However, a large discrepancy was reported in the redox properties between purified proteins and protein complexes in a living cell because the highly reactive enzymes can be easily changed during the purification process.[32] Proteins embedded in a lipid membrane can function together as a whole in the living cell, and their properties should be influenced by a shift in the equilibrium.[32,33] Therefore, a study of in vivo *c*-Cyts will provide more meaningful information that may aid in advancing our understanding of the in situ EET mechanism. Because the active center of *c*-Cyts, heme irons, have a large molar absorption coefficient, spectroscopic methods such as evanescent wave spectroscopy and surface-enhanced infrared absorption have typically been used to investigate the in vivo properties of *c*-Cyts.[18,32,34] An in situ spectroscopic method was also used to study the reaction between Fe^{3+} and *c*-Cyts in intact *Leptospirillum ferrooxidans* under aerobic conditions.[35] In our previous work, we also used UV/visible diffuse-transmittance absorption spectroscopy to monitor the *c*-Cyts in the living cells of bacterial suspensions.[3,22] However, a detailed investigation on the in situ kinetics between the *c*-Cyts and ESs in living bacteria suspensions is still lacking.

In this study, the ES-mediated EET by *Shewanella putrefaciens* 200 (SP200) were investigated in the presence of various ESs with E_h^0 values in the range of −247 mV to −51 mV in MFCs; the objectives were to (i) evaluate the effects of various ESs on electron outputs of SP200 by measuring the current generated; (ii) correlate the electron outputs with the E_h^0 and the EAC of various ESs and establish the quantitative property−activity relationships among electron outputs, E_h^0, EAC, and speciation of ESs; (iii) derive the thermodynamic equations of each elementary reaction during the ES-mediated EET processes from bacteria to an insoluble electron acceptor; and (iv) examine the in situ spectral kinetics of ES reduction in a living SP200 suspension. This study is expected to enhance our fundamental understanding of the electrochemical properties and thermodynamics of various ESs and their influence on the EET in many natural and engineered systems.

EXPERIMENTAL SECTION

Materials. *Shewanella putrefaciens* 200 (SP200) is an iron-reducing bacterium.[36,37] The strain was grown aerobically as batch cultures in LB medium to the midexponential phase and was subsequently used for electrochemical experiments. 2-Hydroxy-1,4-naphthoquinone (2-HNQ, 97%) and 9,10-anthraquinone-2-sulfonic acid (AQS, 98.0%) were purchased from Acros. 9,10-Anthraquinone-2,6-disulfonic acid (AQDS, 98%), 9,10-anthraquinone-2-carboxylic acid (AQC, 99%), resazurin sodium salt (RZ, 90%), and flavin mononucleotide (FMN, 93%) were purchased from TCI (Japan). Riboflavin (RF, 98%) was purchased from Aladdin (China). Other chemicals were of analytical grade and were obtained from Guangzhou Chemical Co. (China).

MFC Configuration and Operation. Double-chamber MFCs were used in this study with schematic and configuration in Supporting Information (SI) Figure S1. A suspension of SP200 in midexponential phase (ca. 10^7 cells mL^{-1}) with ESs (50 μM) in a phosphate buffer solution (0.2 M, pH 7.0) containing lactate (20 mM), mineral solution and vitamin solution[38] was added to the anode chamber, and then it was purged with O_2-free N_2 for at least 30 min before being transferred into an Anaerobic Chamber (DG250, Don Whitley Scientific, England). The anode chamber was sealed with butyl rubber stoppers, and 0.1 M potassium ferricyanide was subsequently added to the opposite chamber as a catholyte and a 1000 Ω resistor was set as an external load. The reactors were taken out of the Anaerobic Chamber and connected with the 32-channel voltage collection instrument (AD8223, China). All experiments were conducted at a controlled temperature of 30 °C. The current was calculated from the obtained voltage and external resistance on the basis of Ohm's law. The polarization, power densities and open-circuit voltages of the MFCs were measured; the experimental details are provided in the SI.[39] Cyclic voltammetry (CV) and EAC measurements were performed using a potentiostat (CHI660D, Chenhua Co., Ltd., Shanghai, China).[28]

In Situ Spectral Measurements of *c*-Cyts and ESs. SP200 was grown aerobically in nutrient broth at 30 °C for 18 h. The suspension was subsequently centrifuged at 7000*g* for 10 min at 4 °C; the pellets were washed three times and then transferred into the Anaerobic Chamber and resuspended in sterile oxygen-free PIPES buffer (1,4-piperazinediethanesulfonic acid, pH 7.0). The cell suspension at a final concentration of 1×10^8 cells mL^{-1} was added to a rectangular quartz cuvette with an optical path length of 1.0 cm, and the cuvette was subsequently sealed and taken out of the Anaerobic Chamber. The control without ES was first measured before ES (0.15 mM) was added, and the spectra were collected at intervals using a UV/visible spectrophotometer (TU-1901 Beijing, China) equipped with an IS19−1 integrating sphere reflectance attachment (22 to 25 °C).[3,22,40] The scanning wavelength range was 300−700 nm. The wavelength of the specific peak of individual ES was 453, 328, and 331 nm for 2-HNQ_{ox}, $AQDS_{ox}$,

dx.doi.org/10.1021/es5017312 | Environ. Sci. Technol. 2014, 48, 9306−9314

Table 1. Average Constant Current (I_{ave}) and Electrochemical Parameters (OCV, P_{max}, and R_{int}) of MFCs in the Absence or Presence of ESs, Standard Redox Potentials (E^0_{ES}), Electron Accepting Capacities (EAC), and log K_{ow} of ESs

parameters	CK	AQC	AQS	FMN	RF	AQDS	2-HNQ	RZ
I_{ave} (mA)	0.222	0.627	0.639	0.619	0.625	0.582	0.534	0.380
OCV (mV)	323	674	699	685	698	658	606	459
P_{max} (mW m^{-2})	206	1016	1335	1095	1271	940	765	375
R_{int} (Ω)	34	70	40	62	47	71	78	101
E^0_{ES} (mV)		−247	−225	−219	−208	−184	−137	−51
EAC ($mmol_e^-(mol_{ES})^{-1}$)		262	212	220	235	199	167	99
log K_{ow}		3.23	0.19	−1.73	−1.46	−0.76	1.38	N/A

and AQS_{ox}, respectively, and the concentrations of ESs were obtained according to the standard curves. While the accurate concentration of *c*-Cyts was not quantified here, the ratios of *c*-Cyt_{red}/*c*-Cyt_{ox} used in the E_h calculation can be directly obtained from the ratios of the peak intensity of *c*-Cyts at 552 nm.

RESULTS AND DISCUSSION

Effects of ESs on Electron Outputs. The results in SI Figure S2 reveal that the current in all the MFC reactors initially increased slowly until 24 h and then sharply reached a constant output after approximately 72 h. To clearly illustrate the differences in the electron outputs, the average current values in the constant stage were calculated; the results, which are summarized in Table 1, suggest that the average constant current (I_{ave}) with and without ESs decreased in the order AQS > AQC > RF > FMN > AQDS > 2-HNQ > RZ > CK (Table 1), where the highest I_{ave} value with AQS was 2.9 times higher than that without an ES and even the lowest I_{ave} value with RZ was 1.7 times higher than that without an ES. These results indicate that the presence of ESs substantially enhanced the electron outputs by the SP200 compared with the control treatment (CK), which is consistent with previous similar studies on iron reduction.[23] As *Shewanella* has the capacity of releasing riboflavin,[41] the supernatant from the SP200 suspension cultured without any ES in the MFC was collected for characterization of potential self-secreted riboflavin by DPVs and UV−vis spectra. Results in SI Figure S3a show that a tiny peak was observed at ∼ −0.2 V (vs SHE) which may represent the self-secreted riboflavin of SP200. However, the peak intensity of this possible self-secreted riboflavin is much lower than that of the exogenous riboflavins with 50 μM. The UV−vis spectra (SI Figure S3b) also show that the absorbance of self-secreted riboflavin was much lower than that of the exogenous riboflavins. Therefore, the influence of self-secreted riboflavin can be ignored.

To compare the electrochemical properties of MFCs with different ESs, the polarization behavior of different MFCs was determined on the 3.5th day of operation. The polarization curves in SI Figure S4a indicate that, although the open-circuit voltage (OCV) of CK was the lowest voltage value, the OCVs of other MFCs in the presence of ESs were substantially higher than that of CK. The OCVs at zero current density are summarized in Table 1 with the ranking order AQS > RF > FMN > AQC > AQDS > 2-HNQ > RZ > CK. The internal resistances (R_{int}) were also obtained by calculating the slope of the voltage vs current production curves (SI Figure S4a); the results are presented in Table 1 and suggest that the order of R_{int} of all of the MFCs was RZ > 2-HNQ > AQDS >AQC > FMN > RF > AQS > CK. Power density curves were also measured (SI Figure S4b), and the maximum power densities (P_{max}) of the MFCs were derived from the peaks; the results presented in Table 1 reveal that the rank order of P_{max} was the same as that for OCV. The P_{max} value with AQS (1335 mW m^{-2}) was 6.5 times greater than that with CK. The polarization behavior of these MFCs clearly demonstrates that the presence of ESs substantially enhanced the current output capacity, as indicated by their observed higher OCV and P_{max}. To clearly illustrate the contribution of the anode and cathode to the overall current generation, the electrode potentials of the anodes and cathodes were also examined. The results in SI Figure S4c indicate that, although the cathode potentials of the various MFCs were consistent, the anode potentials varied substantially in a manner similar to the variation of the overall polarization curves in SI Figure S4a; these variations indicate that the differences in electricity output by SP200 with ESs were mainly attributable to the different anode potentials induced by the ESs.

Impact of E^0_{ES} on ES-Mediated Extracellular Electron Transfer. Because the redox potential (E_h) of ESs is a critical parameter related to thermodynamic control of the ES-mediated extracellular electron transfer process,[21,23] the correlation between the current generated with ESs in MFCs and their standard redox potential (E^0_{ES}) were investigated. The results (Figure 1a) indicate that the I_{ave} decreased gradually as the E^0_{ES} was increased from −247 mV to −51 mV (Table 1); this behavior is also reflected in the cyclic voltammograms (CVs) in SI Figure S5. A high correlation coefficient (R) of 0.973 was obtained from the linear regression fitting of I_{ave} vs E^0_{ES}, which indicates that the I_{ave} was strongly correlated with the E^0_{ES} of ESs. Further analyses were conducted on the correlation between E^0_{ES} and the electrochemical parameters (OCV, P_{max}, and R_{int}) derived from the polarization curves in SI Figure S4. Although the OCV and P_{max} tended to decrease with increasing E^0_{ES}, similar to the case for I_{ave}, the R_{int} increased gradually with increasing E^0_{ES} and strong linear relationships were observed in the plots of OCV vs E^0_{ES} (R = 0.946) (Figure 1b), P_{max} vs E^0_{ES} (R = 0.873) (Figure 1c), and R_{int} vs E^0_{ES} (R = 0.763) (Figure 1d). A similar linear correlation was also observed between E^0_h and the effects of ESs on microbial iron reduction by *Shewanella putrefaciens* CN32, where the iron reduction rates were negatively correlated with the E^0_h of the ESs (−247 mV to 11 mV).[23] Although no linear correlation was observed between E^0_{ES} and the iron reduction rates with ESs in a wide range from −500 mV to −3 mV,[20−22] we nonetheless noted that a decrease similar to that in Figure 1a was obtained when the ESs with E^0_{ES} values in a narrow range of −254 mV to −3 mV were considered. The good correlations between E^0_{ES} and all of the examined parameters (I_{ave}, OCV, P_{max}, and R_{int}) confirmed that the E^0_{ES} of the ESs was a key factor in enhancing the electron output of SP200.

dx.doi.org/10.1021/es5017312 | Environ. Sci. Technol. 2014, 48, 9306−9314

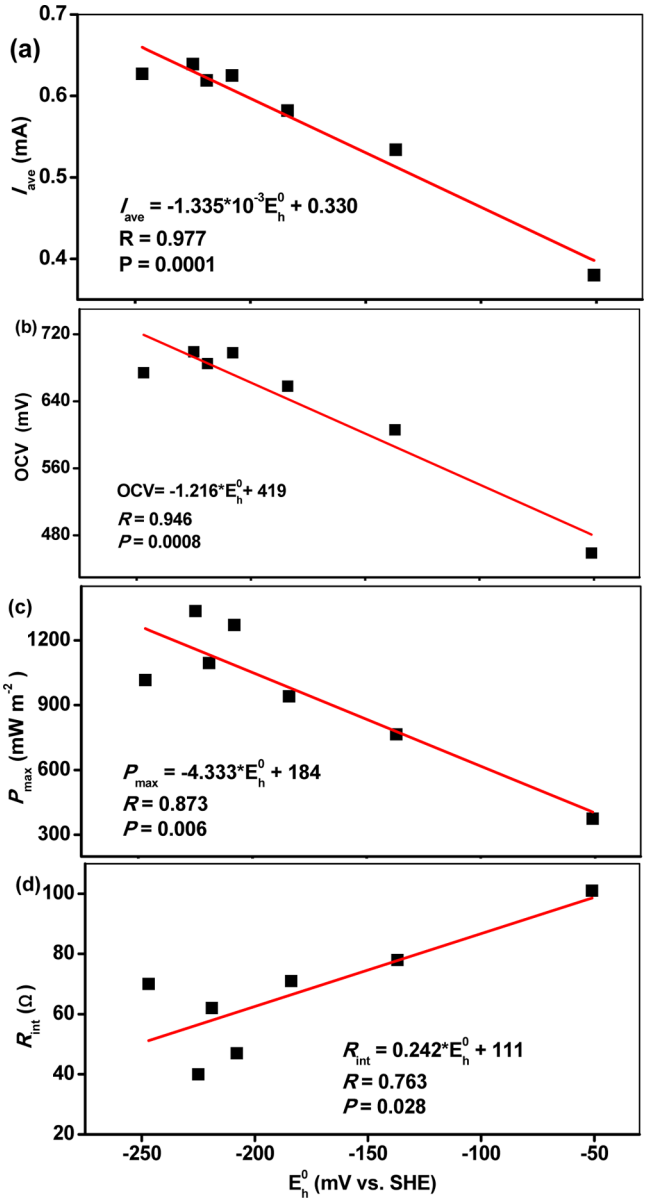

Figure 1. Correlation between the standard redox potentials of ESs (E^0_{ES}) and the electrochemical parameters (a) I_{ave}, (b) OCV, (c) P_{max}, and (d) R_{int}. The data were measured on the 3.5th day of operation, when the current of all the cells reached a stable value and an open circuit was maintained for 4 h.

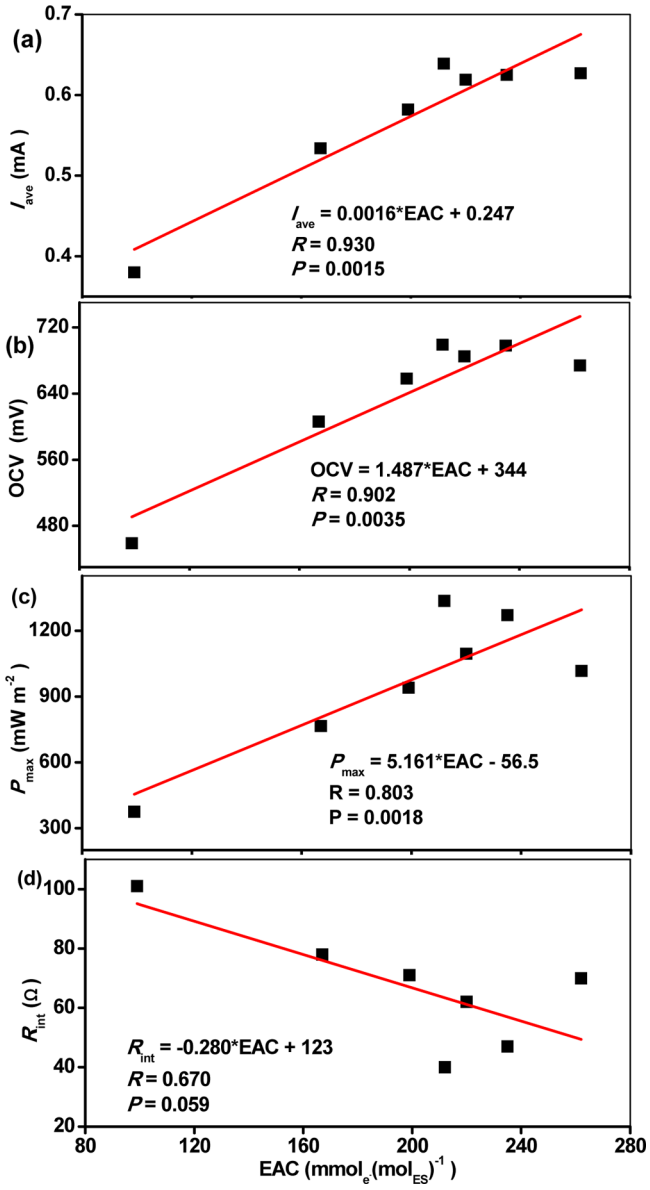

Figure 2. Correlation between the electron accepting capacities (EAC) of ESs and the electrochemical parameters (a) I_{ave}, (b) OCV, (c) P_{max}, and (d) R_{int}. The data were measured on the 3.5th day of operation, when the current of all the cells reached a stable value and an open circuit was maintained for 4 h.

Impact of EAC on ES-Mediated Extracellular Electron Transfer. The relationship between the EAC and iron reduction rates has been previously reported,[20−22] and the results suggest that the ES-mediated microbial iron reduction rates strongly depend on the EAC of those ESs. Here, the EAC of different ESs were determined using amperometric *i*-t measurements in a buffer solution (pH 7.0, phosphate 0.2 M) similar to that used in MFCs. The results in Table 1, which were calculated from the results in SI Figure S6, showed a descending order of AQC > RF > FMN > AQS > AQDS > 2-HNQ > RZ. To clearly illustrate the relationship between the effectiveness of ESs for electron output by SP200 and their EAC, the I_{ave} as a function of EAC was plotted, as presented in Figure 2a. The results revealed that the I_{ave} values correlated well with the EAC of the ESs, as indicated by correlation coefficients (R) as high as 0.930 for the linear regression fitting. These results suggest that the effectiveness of different ESs for enhancing electron outputs is positively associated with the EAC of the ESs. Further analysis of the relationship between the EAC and the electrochemical properties of MFCs with ESs suggested that, although the OCV and P_{max} increased with increasing EAC, the R_{int} decreased gradually with increasing EAC; strong linear relationships were observed in the plots of OCV vs EAC (R = 0.902) (Figure 2b), P_{max} vs EAC (R = 0.803) (Figure 2c), and R_{int} vs EAC (R = 0.670) (Figure 2d). This finding is consistent with those of previous reports,[20−22] which suggests that ES-mediated EET processes are strongly dependent on the EAC of the ESs.

Since transport of ESs into cell or surface reaction of ESs with cytochromes may influence the overall EET processes, the log K_{ow} of ESs was also taken into consideration. While the log K_{ow} values of all the ESs are quite different as shown in Table 1,

dx.doi.org/10.1021/es5017312 | Environ. Sci. Technol. 2014, 48, 9306−9314

no good linear correlation was observed between log K_{ow} and I_{ave} (SI Figure S7). According to the calibration of results obtained at 552 nm from UV/vis spectra of cell suspension (SI Figure S13) using cytochrome *c* from equine heart (Sigma, C2506, ε_{550} = 25.68 mM^{-1}), the total cytochrome concentration in cell suspension was estimated as 1−1.5 μM (hemes), which was much less than that of ESs (50 μM), and hence, the log K_{ow} of ESs may just have very limited influence on the overall EET processes.

As the MFCs experiments were conducted with an external resistor of 1000 ohm, the effective anode potential may be different leading to a changing kinetics of ES reoxidation. To further prove the reported phenomenon in Figures 1 and 2, the experiments were performed under galvanostatic condition with the details of schematic and configuration in SI Figure S8. As the current is fixed, the voltage outputs will reflect the difference in the electrode potential caused by the presence of ESs. Results in SI Figure S9 also showed a linear correlation between the electrode potentials and E^0_{ES} (and EAC), which was consistent with the results from the MFCs experiments (Figures 1 and 2). Therefore, the impact of E^0_{ES} and EAC of ESs on the extracellular electron transfer of SP200 can be well verified.

Thermodynamics of ES-Mediated Extracellular Electron Transfer. On the basis of the aforementioned electrode potentials in SI Figure S4c, the difference among the treatments with various ESs is attributed to their different anode potentials; hence, thermodynamic analysis of the reactions that occur at the anode will be useful for revealing the electron transfer mechanisms during the ES-mediated electron outputs. According to Picardal et al.,[42] the *c*-Cyts are the predominant cytochromes present in the outer-membranes of SP200, and a 91-kDa heme-containing protein was found in the OM of SP200.[43] To further investigate the chemical properties of the OM *c*-Cyts of SP200, the outer-membrane proteins have been extracted and similar patterns of oxidized (*c*-Cyt_{ox}) and reduced *c*-Cyts (*c*-Cyt_{red}) were observed in the UV/vis diffuse-transmittance spectra of whole cell and extracted OM proteins of SP200 (SI Figure S12a). The spectroelectrochemical spectra of the extracted OM proteins characterized in a range of potentials spanning between 0 mV and −500 mV (SI Figure S12b), reveal that the *c*-Cyt_{ox} was transformed to the *c*-Cyt_{red} with decreasing external potential. After AQDS was added to the reduced OM proteins, the peak intensity at 552 nm rapidly decreased, indicating that the reaction between *c*-Cyt_{red} and AQDS occurred. Therefore, this result can provide a direct evidence for the electron transfer from *c*-Cyt_{red} to ESs.

The riboflavin-mediated current generation was investigated[44] by using S. *oneidensis* MR-1 with wild type and deletion mutants with results that the current generation with the ΔmtrC, ΔmtrA, ΔmtrB, and ΔomcA/mtrC deletion mutants decreased greatly as compared with that with wild type, suggesting the involvement of *c*-Cyts in the EET of *Shewanella* species. In addition, the current generation by S. *oneidensis* MR-1 decreased rapidly in the presence of metabolic inhibitor (2-heptyl 4hydroxyquinolineN-oxide) for Mtr pathway,[45] further reflecting the involvement of *c*-Cyts. Therefore, in an anode chamber with SP200 and ESs, the electron transfer pathway can be divided into three steps: (i) the intracellular electron transport (IET) from an electron donor to the OM, (ii) the extracellular electron transfer (EET) from OM *c*-Cyts to exogenous ESs, and (iii) the diffusion of reduced ESs to the electrode (anode). The step-by-step potential losses can drive the electron flow from the electron donor to the anode, resulting in the electron output (current).

In Step (i), the electron donor (lactate) can be utilized by SP200 and result in concomitant enrichment of the SP200 cells (eq 1):

$$\text{SP200} + \text{lactate}^- \rightarrow (\text{SP200})_n + \text{acetate}^- + CO_2 + H^+ \quad (1)$$

Because the utilization of an electron donor by bacterium is considered to be the power source of electron flow in MFCs, the anode potential is determined by the following half-cell reaction (eq 2):

$$C_3H_5O_3^- + 2H_2O \rightarrow C_2H_3O_2^- + HCO_3^- + 5H^+ + 4e^- \quad (2)$$

Hence, the specific theoretical anode potential can be calculated on the basis of the standard redox potential of lactate and the concentrations of each species via the Nernst equation. Herein, the influence of ESs on the electron-donor utilization was expected to be similar for all of the MFCs (with or without an ES) because the initial cell density and lactate concentration were identical for all of the MFCs. Results in SI Figure S10 also confirmed that no significant difference of cell density was observed between the treatments with and without ESs, though the biofilm growth was observed on the anode electrode (SI Figure S11). Hence, the potential losses in Step (i) can be assumed to be similar for all of the MFCs with or without an ES.

In Step (ii), because of the existence of potential loss between the electron-donor potential ($E_{lactate}$) and the potential of the outer membrane (OM), the electrons are released from the OM of the cells into OM *c*-Cyts, resulting in an electron sink on the *c*-Cyts.[46] Hence, the oxidized *c*-Cyts (*c*-Cyt_{ox}) are transformed into reduced *c*-Cyts (*c*-Cyt_{red}) via the reduction by the electrons generated by the process in eq 2. For convenience, a two-electron reaction was assumed in thermodynamic calculations, as shown in eq 3:

$$c\text{-}Cyt_{ox} + 2e^- \leftrightarrow c\text{-}Cyt_{red} \quad (3)$$

The *c*-Cyt_{red} can directly transfer electrons to electrodes when the OM is in contact with anode, which is a basic mechanism for the biofilm cases. However, after the addition of ESs, the *c*-Cyt_{red} is readily captured by the soluble oxidized ES (ES_{ox}), which results in the generation of reduced ES (ES_{red}) via eq 4, the ES_{red} can attract the electrons from the OM of the cells (especially the cells located away from the anode surface) to the electrode, resulting in the exogenous ES-mediated EET processes:

$$c\text{-}Cyt_{red} + ES_{ox} \leftrightarrow c\text{-}Cyt_{ox} + ES_{red} \quad (4)$$

where the two-electron reaction for ES reduction is assumed, and the half-cell reaction can be written as eq 5:

$$ES_{ox} + 2e^- \leftrightarrow ES_{red} \quad (5)$$

The specific redox potentials of the *c*-Cyts and ESs ($E_{c\text{-}Cyt}$ and E_{ES}) can be calculated by the Nernst equations presented in eqs 6 and 7:

$$E_{c\text{-}Cyt} = E^0_{c\text{-}Cyt} - \frac{RT}{2F}\ln\frac{[c\text{-}Cyt_{red}]}{[c\text{-}Cyt_{ox}]} \quad (6)$$

dx.doi.org/10.1021/es5017312 | Environ. Sci. Technol. 2014, 48, 9306−9314

$$E_{ES} = E^0_{ES} - \frac{RT}{2F}\ln\frac{[ES_{red}]}{[ES_{ox}]} \quad (7)$$

where R is the ideal gas constant (8.3145 J mol^{-1} K^{-1}); F is the Faraday constant (96 485 C mol^{-1} e$^-$); T is the temperature (K).; and E^0_{c-Cyt} represents the standard redox potentials of the c-Cyts, which have been previously reported in the range of −400 mV to 0 mV.[25,47−50] The standard redox potentials of the ESs (E^0_{ES}) are presented in Table 1. The potential loss (ΔE) between the c-Cyts and the ESs is equal to ($E_{c\text{-}Cyt} - E_{ES}$). Combining $\Delta E = E_{c\text{-}Cyt} - E_{ES}$ with eq 6 and eq 7, we can express the ΔE as eq 8:

$$\Delta E = E^0_{c\text{-}Cyt} - E^0_{ES} - \frac{RT}{2F}\ln\frac{[c\text{-}Cyt_{red}][ES_{ox}]}{[c\text{-}Cyt_{ox}][ES_{red}]} \quad (8)$$

In Step (iii), the interaction between ES_{red} and the anode is described as ES_{red} diffusion to the anode surface followed by electron transfer from ES_{red} to the anode, resulting in the generation of current (eq 9):

$$ES_{red} + \text{anode} \rightarrow \text{anode}\cdot ES_{red} \rightarrow ES_{ox} + \text{current} \quad (9)$$

Although the electron transfer from ES_{red} to the anode is very fast when they are in contact,[51] the transport of soluble ES_{red} to the anode is a slow diffusion process governed by Fick's law.[46] The diffusion of ES_{red} to the electrode can be calculated as eq 10:

$$j = nF\left(\frac{D_{ES}\Delta[ES_{red}]}{\Delta z}\right) \quad (10)$$

where j is the current density (A m^{-2}) obtained using SP200, D_{ES} is the diffusion coefficient of the ES (m^2 s^{-1}), Δz is the transport distance (m), $\Delta[ES_{red}]$ is the concentration gradient of ES_{red} (mol m^{-3}), and nF converts from moles to coulombs. The diffusion coefficients of organic molecules are relatively small and can assumed to be similar for all of the ESs;[52] hence, no great differences were observed among the various ESs with respect to Step (iii).

On the basis of the previous discussion, the IET from an electron donor to an OM (Step (i)) and the diffusion of reduced ESs to the electrode (Step (iii)) can be assumed to be similar for all of the MFCs with or without ESs; hence, the EET from the OM c-Cyts to exogenous ESs (Step (ii)) is a critical step that is responsible for the differences in the overall output of electrons by SP200 in the presence of different ESs.

As evident from eq 8, the potential loss from the OM c-Cyts to the ES is not only determined by the E^0_{c-Cyt} and E^0_{ES}, but is also influenced by the speciation of c-Cyts and ESs (([c-Cyt_{red}][ES_{ox}])/([c-Cyt_{ox}][ES_{red}])). The E^0_{c-Cyt} value can be assumed to be the same for all of the treatments with or without ESs because the same bacteria with the same cell density were used in all of the treatments. Therefore, the variables in eq 8 include E^0_{ES} and the speciation of c-Cyts and ESs. The results in Figure 1 indicate that the current generation (I_{ave}) and polarization parameters (OCV, P_{max}, and R_{int}) are linearly correlated with E^0_{ES}, which reveals that the differences in E^0_{ES}among the ESs may result in a different potential loss (ΔE) and further influence the EET efficiency from SP200 cells to the electrode. In addition, the results in Figure 2 reveal that the current generation (I_{ave}) and polarization parameters (OCV, P_{max}, and R_{int}) are also correlated with the EAC of ESs, which can be calculated according to the following equation (eq 11):

$$EAC = \frac{n_{e^-}}{[ES_{tot}]} = \frac{\sum_i [ES_i]}{[ES_{tot}]} \quad (11)$$

Here, if only two forms of ES (ES_{red} and ES_{ox}) are assumed, the EAC can be simplified as eq 12:

$$EAC = \frac{[ES_{red}]}{[ES_{tot}]} = \frac{[ES_{red}]}{[ES_{red}] + [ES_{ox}]} = \frac{1}{1 + \frac{[ES_{ox}]}{[ES_{red}]}} \quad (12)$$

where [ES_{tot}] represents the total concentration of ES and n_{e^-} represents the total amount of accepting electrons. The equations (eqs 8 and 12) and results in Figure 2 confirm that the speciation of c-Cyts and ESs can directly induce different potential losses (ΔE) and further influence the EET efficiency from the SP200 cells to the electrode. Therefore, the ES-mediated EET process is expected to be directly determined by the kinetics of the c-Cyts and ES species.

In Situ Spectral Analysis of ES Reduction in a Living Cell Suspension. Because Step (ii) is presumed to be the critical step during the electron transfer from the electron donor via the OM c-Cyts and ESs to the electrode and, simultaneously, Step (i) and Step (iii) are presumed to be similar for all of the treatments under the specific conditions used in this study, we first investigated the in situ spectral kinetic analysis of ES reduction in a living SP200 suspension to further illustrate the relationship between the thermodynamic changes and kinetics of the species of c-Cyts and ESs. We performed this investigation by measuring the spectral changes of c-Cyts and ESs simultaneously. Here, three ESs (2-HNQ, AQDS, and AQS) were selected because these three ESs are easily measured by UV/Visible spectroscopy. Their spectra are distinct (SI Figure S13) and contain specific peaks at 453 nm (2-HNQ_{ox}), 328 nm ($AQDS_{ox}$), 331 nm (AQS_{ox}), and 552 nm (c-Cyt_{red}). The combination of individual spectra of c-Cyts and ESs by calculation resulted in a spectrum similar to those of the real mixture of SP200 and ESs, thereby indicating that the concentrations of c-Cyts and ESs can be obtained from their individual peak intensities. The results in SI Figure S14 show the spectral changes of three selected ESs in the SP200 suspension that occurred as time elapsed; the spectra of c-Cyts are presented as well. The intensities of the peaks at 453 nm (2-HNQ_{ox}), 328 nm ($AQDS_{ox}$), 331 nm (AQS_{ox}), and 552 nm (c-Cyt_{red}) were extracted, and the kinetics was plotted in SI Figure S15. The results indicate that the concentrations of all three ESs decreased quickly with time, thereby confirming the effective ES reduction by the SP200. In the case of the OM c-Cyts, although the c-Cyt_{red} sharply decreased from ∼0.03 to 0.01−0.015 at the beginning (first min), the c-Cyt_{red} increased gradually thereafter, indicating that the c-Cyt_{red} reacted with ESs very rapidly at the beginning of the reactions but the electrons were then refilled to the c-Cyt_{ox} via IET, which resulted in a subsequent increase in the c-Cyt_{red} concentrations.

Because the speciation of c-Cyts and ESs are critical for the ΔE in eq 8 and the EAC in eq 12, the natural logarithm values of [c-Cyt_{red}]/[c-Cyt_{ox}], [ES_{ox}]/[ES_{red}], and ([c-Cyt_{red}] [ES_{ox}])/([c-Cyt_{ox}][ES_{red}]) were calculated and the specific redox potentials of c-Cyts ($E_{c\text{-}Cyt}$) and ESs (E_{ES}) as well as the potential losses (ΔE) were obtained from eqs 6 − 8. Because the values of E^0_{c-Cyt} in the wide range of −400 mV to 0 mV have been previously reported,[25,47,48] a value of −0.25 V (vs SHE) can be reasonably used here for the calculation of specific E values ($E_{c\text{-}Cyt}$ and ΔE). Results in Figure 3a reveal that the $E_{c\text{-}Cyt}$ in the presence of ESs decreased gradually with time, which is

dx.doi.org/10.1021/es5017312 | Environ. Sci. Technol. 2014, 48, 9306−9314

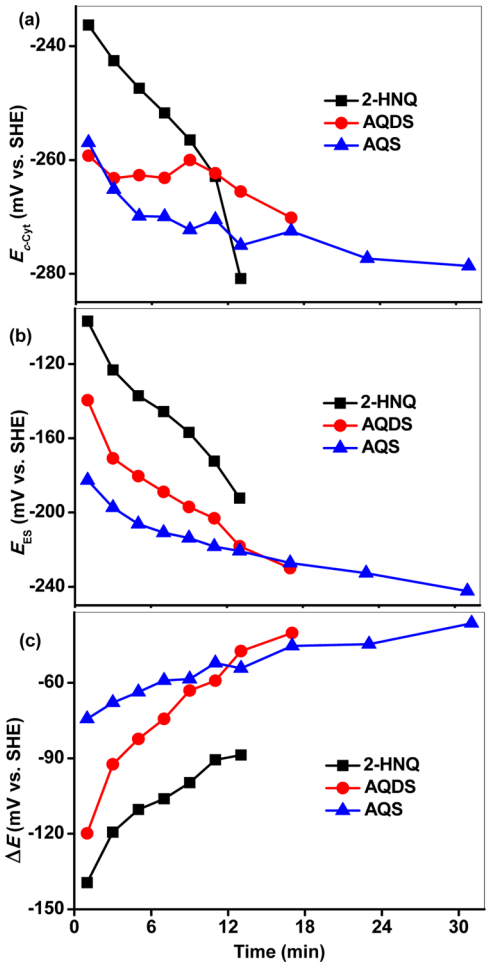

Figure 3. Calculated E_h values of *c*-Cyts (a), ESs (2-HNQ, AQDS, and AQS) (b) and the potential loss (ΔE) (c) in terms of eqs 7, 8, and 9. The natural logarithm values of [*c*-Cyt_{red}]/[*c*-Cyt_{ox}], [ES_{ox}]/[ES_{red}], and ([*c*-Cyt_{red}] [ES_{ox}])/([*c*-Cyt_{ox}][ES_{red}]) as functions of time were calculated from the individual concentrations of each species in SI Figure S15. The E^0_{ES} of ESs were obtained from Table 1, and the E^0_{c-Cyt} was estimated to be −0.25 V (vs SHE) according to previously reported values.[25,47,48]

attributed to the regeneration of *c*-Cyt_{red} via intracellular electron transfer process, but the $E_{c\text{-Cyt}}$ decreased very slightly (from −240 mV to −280 mV) due to the simultaneous reoxidation of *c*-Cyt_{red} by ESs. The E_{ES} of the three tested ESs in Figure 3b decreased with elapsed time because of the direct reduction by *c*-Cyt_{red} and were ranked as an order of 2-HNQ > AQDS > AQS, which is consistent the order of E^0_{ES}in Table 1. The potential losses (ΔE) in Figure 3c for three ESs increased with time, indicating that the driving force of the reaction between the *c*-Cyt_{red} and ES_{ox} decreased as the reaction proceeded. As the potential loss can lead to a positive-shift of overall potential, the more positive anode potential (SI Figure S4c) was observed for 2-HNQ with the lowest ΔE value (Figure 3c).

Although the generation of constant current in MFCs can be attributed to the redox equilibrium for all of the electron transfer processes, including Steps (i), (ii), and (iii), the redox reactions of the ESs in the living SP200 suspension still differed substantially from the equilibrium state because the experiments were conducted in a short time (<30 min); moreover, no electrode was used because as a terminal electron acceptor in the reaction system, resulting in the electron transfer simply ceasing at the ES_{red}. However, the aforementioned discussion first provided a quantitative analysis of the relationship between the potential loss of EET and the speciation of *c*-Cyts and ESs. Future work will be very worthwhile to comprehensively understand the relationship between the kinetics of redox species and the specific redox potentials via the combination of thermodynamic calculations and the in situ spectral analyses of the speciation of *c*-Cyts and ESs.

Environmental Implications. A number of ESs or ES-bearing natural organic materials have been reported to be involved in many EET processes, including microbial electricity generation, biogeochemical cycling of redox-active elements, and contaminant transformations.[16] While the finding that the presence of ESs can significantly facilitate electricity generation by a dissimilatory iron reducing bacteria (DIRB), the ES-mediated EET mechanism during electricity generation can also be analogous to many other systems with electron outputs by DIRB, particularly in anoxic environments (e.g., microbial metal reduction, biodegradation of organic chlorinated compounds, carbon cycling and greenhouse gas formation).[53−55] The linear correlation between the electrical parameters (I_{ave}, OCV, P_{max}, and R_{int}) and the E^0_{ES} and EAC highlighted the critical roles of electrochemical properties of ESs in shuttling EET processes and implied that various ESs in natural environments contribute to natural biogeochemical redox processes to different extents.[17] Whereas most previous studies focused on the kinetic aspects of ES-mediated EET processes,[51,56−59] only a few studies related to the potential loss in the EET processes[46] from a thermodynamic viewpoint have been reported. However, detailed theoretical studies on the redox potentials of both ESs and *c*-Cyts (E_{ES} and $E_{c\text{-Cyts}}$) as well as the potential losses (ΔE) provide a molecular-level understanding of the ES-mediated EET processes; furthermore, increased understanding of the critical steps controlling the relative importance of these mechanisms will help in the development of bioremediation strategies and in the prediction of natural attenuation processes.[60,61] The in situ spectral kinetic analysis of ES reduction in a living SP200 suspension provided a direct method of examining the ESs and *c*-Cyts simultaneously, and this method was used to calculate the theoretical redox potential according to the thermodynamic calculation equations related to the E_{ES}, $E_{c\text{-Cyts}}$, and ΔE; thus, the correlation between kinetic and thermodynamic analyses were established. This approach will help advance quantitative models describing the reactivity and capacity of contaminant fate and transport at the field scale.[62,63]

■ ASSOCIATED CONTENT

Supporting Information

Additional data can be found in the Supporting Information including the Figures S1−15 and Table S1 with illustrations. This material is available free of charge via the Internet at http://pubs.acs.org.

■ AUTHOR INFORMATION

Corresponding Authors

*Phone:+86 20 87024721; fax: +86 20 87024123; e-mail; txliu@soil.gd.cn.

*E-mail: cefbli@soil.gd.cn

Notes

The authors declare no competing financial interest.

■ ACKNOWLEDGMENTS

This work was funded by the National Natural Science Foundations of China (nos. 41340018, 41330857, and 41025003) and the Natural Science Foundation of Guangdong Province, China (S2011030002882). We acknowledge three anonymous reviewers for constructive comments, and we are also grateful to Professor Gary S. Sayler at University of Tennessee, who served as Associate Editor, for his fair and timely handling of this manuscript.

■ REFERENCES

(1) Lovley, D. R.; Coates, J. D.; Blunt-Harris, E. L.; Phillips, E. J.; Woodward, J. C. Humic substances as electron acceptors for microbial respiration. *Nature* **1996**, *382*, 445−448.
(2) Logan, B. E.; Regan, J. M. Microbial fuel cells-challenges and applications. *Environ. Sci. Technol.* **2006**, *40*, 5172−5180.
(3) Liu, T. X.; Li, X. M.; Zhang, W.; Hu, M.; Li, F. B. Fe (III) oxides accelerate microbial nitrate reduction and electricity generation by *Klebsiella pneumoniae* L17. *J. Colloid Interface Sci.* **2014**, *423*, 25−32.
(4) Gralnick, J. A.; Newman, D. K. Extracellular respiration. *Mol. Microbiol.* **2007**, *65*, 1−11.
(5) Bird, L. J.; Bonnefoy, V.; Newman, D. K. Bioenergetic challenges of microbial iron metabolisms. *Trends Microbiol.* **2011**, *19*, 330−340.
(6) Stams, A. J.; De Bok, F. A.; Plugge, C. M.; Eekert, V.; Miriam, H.; Dolfing, J.; Schraa, G. Exocellular electron transfer in anaerobic microbial communities. *Environ. Microbiol.* **2006**, *8*, 371−382.
(7) Lovley, D. R. Electromicrobiology. *Annu. Rev. Microbiol.* **2012**, *66*, 391−409.
(8) Yang, Y. G.; Xu, M. Y.; Guo, J.; Sun, G. P. Bacterial extracellular electron transfer in bioelectrochemical systems. *Process Biochem.* **2012**, *47*, 1707−1714.
(9) Brutinel, E. D.; Gralnick, J. A. Shuttling happens: Soluble flavin mediators of extracellular electron transfer in *Shewanella*. *Appl. Microbiol. Biotechnol.* **2012**, *93*, 41−48.
(10) Roller, S. D.; Bennetto, H. P.; Delaney, G. M.; Mason, J. R.; Stirling, J. L.; Thurston, C. F. Electron-transfer coupling in microbial fuel cells: 1. Comparison of redox-mediator reduction rates and respiratory rates of bacteria. *J. Chem. Technol. Biotechnol.* **1984**, *34*, 3−12.
(11) Marsili, E.; Baron, D. B.; Shikhare, I. D.; Coursolle, D.; Gralnick, J. A.; Bond, D. R. *Shewanella* secretes flavins that mediate extracellular electron transfer. *Proc. Natl. Acad. Sci. U.S.A.* **2008**, *105*, 3968−3973.
(12) Newman, D. K.; Kolter, R. A role for excreted quinones in extracellular electron transfer. *Nature* **2000**, *405*, 94−97.
(13) Hernandez, M.; Newman, D. K. Extracellular electron transfer. *Cell. Mol. Life Sci.* **2001**, *58*, 1562−1571.
(14) Li, F. B.; Li, X. M.; Zhou, S. G.; Zhuang, L.; Cao, F.; Huang, D. Y.; Xu, W.; Liu, T. X.; Feng, C. H. Enhanced reductive dechlorination of DDT in an anaerobic system of dissimilatory iron-reducing bacteria and iron oxide. *Environ. Pollut.* **2010**, *158*, 1733−1740.
(15) Cao, F.; Liu, T. X.; Wu, C. Y.; Li, F. B.; Li, X. M.; Yu, H. Y.; Tong, H.; Chen, M. J. Enhanced biotransformation of DDTs by an iron-and humic-reducing bacteria *Aeromonas hydrophila* HS01 upon addition of goethite and anthraquinone-2, 6-disulphonic disodium salt (AQDS). *J. Agric. Food Chem.* **2012**, *60*, 11238−11244.
(16) Brose, D. A.; James, B. R. Oxidation - reduction transformations of chromium in aerobic soils and the role of electron-shuttling quinones. *Environ. Sci. Technol.* **2010**, *44*, 9438−9444.
(17) Borch, T.; Kretzschmar, R.; Kappler, A.; Cappellen, P. V.; Ginder-Vogel, M.; Voegelin, A.; Campbell, K. Biogeochemical redox processes and their impact on contaminant dynamics. *Environ. Sci. Technol.* **2009**, *44*, 15−23.
(18) Liu, T. X.; Li, X. M.; Li, F. B.; Zhang, W.; Chen, M. J.; Zhou, S. G. Reduction of iron oxides by *Klebsiella pneumoniae* L17: Kinetics and surface properties. *Colloid. Surf. A* **2011**, *379*, 143−150.
(19) Aeschbacher, M.; Vergari, D.; Schwarzenbach, R. P.; Sander, M. Electrochemical analysis of proton and electron transfer equilibria of the reducible moieties in humic acids. *Environ. Sci. Technol.* **2011**, *45*, 8385−8394.
(20) Li, X. M.; Liu, L.; Liu, T. X.; Yuan, T.; Zhang, W.; Li, F. B.; Zhou, S. G.; Li, Y. T. Electron transfer capacity dependence of quinone-mediated Fe (III) reduction and current generation by *Klebsiella pneumoniae* L17. *Chemosphere* **2013**, *92*, 218−224.
(21) Wolf, M.; Kappler, A.; Jiang, J.; Meckenstock, R. U. Effects of humic substances and quinones at low concentrations on ferrihydrite reduction by *Geobacter metallireducens*. *Environ. Sci. Technol.* **2009**, *43*, 5679−5685.
(22) Li, X. M.; Liu, T. X.; Liu, L.; Li, F. B. Dependence of the electron transfer capacity on the kinetics of quinone-mediated Fe (iii) reduction by two iron/humic reducing bacteria. *RSC Adv.* **2014**, *4*, 2284−2290.
(23) O'Loughlin, E. J. Effects of electron transfer mediators on the bioreduction of lepidocrocite (γ-FeOOH) by *Shewanella putrefaciens* CN32. *Environ. Sci. Technol.* **2008**, *42*, 6876−6882.
(24) Liu, Y.; Kim, H.; Franklin, R. R.; Bond, D. R. Linking spectral and electrochemical analysis to monitor *c*-type cytochrome redox status in living *Geobacter sulfurreducens* biofilms. *ChemPhysChem* **2011**, *12*, 2235−2241.
(25) Hartshorne, R. S.; Reardon, C. L.; Ross, D.; Nuester, J.; Clarke, T. A.; Gates, A. J.; Mills, P. C.; Fredrickson, J. K.; Zachara, J. M.; Shi, L. Characterization of an electron conduit between bacteria and the extracellular environment. *Proc. Natl. Acad. Sci. U.S.A.* **2009**, *106*, 22169−22174.
(26) Bauer, M.; Heitmann, T.; Macalady, D. L.; Blodau, C. Electron transfer capacities and reaction kinetics of peat dissolved organic matter. *Environ. Sci. Technol.* **2007**, *41*, 139−145.
(27) Blodau, C.; Bauer, M.; Regenspurg, S.; Macalady, D. Electron accepting capacity of dissolved organic matter as determined by reaction with metallic zinc. *Chem. Geol.* **2009**, *260*, 186−195.
(28) Aeschbacher, M.; Sander, M.; Schwarzenbach, R. P. Novel electrochemical approach to assess the redox properties of humic substances. *Environ. Sci. Technol.* **2009**, *44*, 87−93.
(29) Qian, X. L.; Mester, T.; Morgado, L.; Arakawa, T.; Sharma, M. L.; Inoue, K.; Joseph, C.; Salgueiro, C. A.; Maroney, M. J.; Lovley, D. R. Biochemical characterization of purified OmcS, a *c*-type cytochrome required for insoluble Fe (III) reduction in *Geobacter sulfurreducens*. *Biochim. Biophys. Acta, Bioenerg.* **2011**, *1807*, 404−412.
(30) Morris, C. J.; Black, A.; Pealing, S. L.; Manson, F.; Chapman, S. K.; Reid, G.; Gibson, D. M.; Ward, F. B. Purification and properties of a novel cytochrome: Flavocytochrome c from *Shewanella putrefaciens*. *Biochem. J.* **1994**, *302*, 587−593.
(31) Ross, D. E.; Brantley, S. L.; Tien, M. Kinetic characterization of OmcA and MtrC, terminal reductases involved in respiratory electron transfer for dissimilatory iron reduction in *Shewanella oneidensis* MR-1. *Appl. Environ. Microbiol.* **2009**, *75*, 5218−5226.
(32) Nakamura, R.; Ishii, K.; Hashimoto, K. Electronic absorption spectra and redox properties of c type cytochromes in living microbes. *Angew. Chem., Int. Ed.* **2009**, *48*, 1606−1608.
(33) Tributsch, H.; Pohlmann, L. Electron transfer: Classical approaches and new frontiers. *Science* **1998**, *279*, 1891−1895.
(34) Busalmen, J. P.; Esteve-Nuñez, A.; Berná, A.; Feliu, J. M. ATR-SEIRAs characterization of surface redox processes in *G. sulfurreducens*. *Bioelectrochemistry* **2010**, *78*, 25−29.
(35) Blake, R. C., II; G, M. N. *In situ* spectroscopy on intact *Leptospirillum ferrooxidans* reveals that reduced cytochrome 579 is an obligatory intermediate in the aerobic iron respiratory chain. *Front. Microbiol.* **2012**, *3*, 144−153.
(36) DiChristina, T. J. Effects of nitrate and nitrite on dissimilatory iron reduction by *Shewanella putrefaciens* 200. *J. Bacteriol.* **1992**, *174*, 1891−1896.
(37) Park, D.; Zeikus, J. Impact of electrode composition on electricity generation in a single-compartment fuel cell using *Shewanella putrefaciens*. *Appl. Microbiol. Biotechnol.* **2002**, *59*, 58−61.
(38) Li, X. M.; Zhou, S. G.; Li, F. B.; Wu, C. Y.; Zhuang, L.; Xu, W.; Liu, L. Fe (III) oxide reduction and carbon tetrachloride

dechlorination by a newly isolated *Klebsiella pneumoniae* strain L17. *J. Appl. Microbiol.* **2009**, *106*, 130−139.
(39) Logan, B. E.; Hamelers, B.; Rozendal, R.; Schröder, U.; Keller, J.; Freguia, S.; Aelterman, P.; Verstraete, W.; Rabaey, K. Microbial fuel cells: Methodology and technology. *Environ. Sci. Technol.* **2006**, *40*, 5181−5192.
(40) Zhang, W.; Li, X. M.; Liu, T. X.; Li, F. B.; Shen, W. J. Competitive reduction of nitrate and iron oxides by *Shewanella putrefaciens* 200 under anoxic conditions. *Colloid. Surf., A* **2014**, *445*, 97−104.
(41) Von Canstein, H.; Ogawa, J.; Shimizu, S.; Lloyd, J. R. Secretion of flavins by *Shewanella* species and their role in extracellular electron transfer. *Appl. Environ. Microbiol.* **2008**, *74*, 615−623.
(42) Picardal, F. W.; Arnold, R. G.; Couch, H.; Little, A. M.; Smith, M. E. Involvement of cytochromes in the anaerobic biotransformation of tetrachloromethane by *Shewanella putrefaciens* 200. *Appl. Environ. Microbiol.* **1993**, *59*, 3763−3770.
(43) DiChristina, T. J.; Moore, C. M.; Haller, C. A. Dissimilatory Fe (III) and Mn (IV) reduction by *Shewanella putrefaciens* requires ferE, a homolog of the pulE (gspE) type II protein secretion gene. *J. Bacteriol.* **2002**, *184*, 142−151.
(44) Coursolle, D.; Baron, D. B.; Bond, D. R.; Gralnick, J. A. The Mtr respiratory pathway is essential for reducing flavins and electrodes in *Shewanella oneidensis*. *J. Bacteriol.* **2010**, *192*, 467−474.
(45) Okamoto, A.; Hashimoto, K.; Nealson, K. H.; Nakamura, R. Rate enhancement of bacterial extracellular electron transport involves bound flavin semiquinones. *Proc. Natl. Acad. Sci. U.S.A.* **2013**, *110*, 7856−7861.
(46) Torres, C. I.; Marcus, A. K.; Lee, H. S.; Parameswaran, P.; Krajmalnik-Brown, R.; Rittmann, B. E. A kinetic perspective on extracellular electron transfer by anode-respiring bacteria. *FEMS Microbiol. Rev.* **2009**, *34*, 3−17.
(47) Firer-Sherwood, M.; Pulcu, G. S.; Elliott, S. J. Electrochemical interrogations of the Mtr cytochromes from *Shewanella*: Opening a potential window. *J. Biol. Inorg. Chem.* **2008**, *13*, 849−854.
(48) Clarke, T. A.; Edwards, M. J.; Gates, A. J.; Hall, A.; White, G. F.; Bradley, J.; Reardon, C. L.; Shi, L.; Beliaev, A. S.; Marshall, M. J. Structure of a bacterial cell surface decaheme electron conduit. *Proc. Natl. Acad. Sci. U.S.A.* **2011**, *108*, 9384−9389.
(49) Akutsu, H.; Takayama, Y. Functional roles of the heme architecture and its environment in tetraheme cytochrome c. *Acc. Chem. Res.* **2007**, *40*, 171−178.
(50) Bewley, K. D.; Ellis, K. E.; Firer-Sherwood, M. A.; Elliott, S. J. Multi-heme proteins: Nature's electronic multi-purpose tool. *Biochim. Biophys. Acta* **2013**, *1827*, 938−948.
(51) Jiang, J.; Kappler, A. Kinetics of microbial and chemical reduction of humic substances: Implications for electron shuttling. *Environ. Sci. Technol.* **2008**, *42*, 3563−3569.
(52) Lide, D. R. *CRC Handbook of Chemistry and Physics*; CRC press, 2004.
(53) Van der Zee, F. P.; Cervantes, F. J. Impact and application of electron shuttles on the redox (bio) transformation of contaminants: A review. *Biotechnol. Adv.* **2009**, *27*, 256−277.
(54) Plymale, A. E.; Bailey, V. L.; Fredrickson, J. K.; Heald, S. M.; Buck, E. C.; Shi, L.; Wang, Z.; Resch, C. T.; Moore, D. A.; Bolton, H., Jr. Biotic and abiotic reduction and solubilization of Pu (IV) O_2• x H_2O $_{(am)}$ as affected by anthraquinone-2, 6-disulfonate (AQDS) and ethylenediaminetetraacetate (EDTA). *Environ. Sci. Technol.* **2012**, *46*, 2132−2140.
(55) Klüpfel, L.; Piepenbrock, A.; Kappler, A.; Kappler, A.; Sander, M. Humic substances as fully regenerable electron acceptors in recurrently anoxic environments. *Nat. Geosci.* **2014**, *7*, 195−200.
(56) Turick, C. E.; Tisa, L. S.; Caccavo, F., Jr. Melanin production and use as a soluble electron shuttle for Fe (III) oxide reduction and as a terminal electron acceptor by *Shewanella algae* BrY. *Appl. Environ. Microbiol.* **2002**, *68*, 2436−2444.
(57) McKinlay, J. B.; Zeikus, J. G. Extracellular iron reduction is mediated in part by neutral red and hydrogenase in *Escherichia coli*. *Appl. Environ. Microbiol.* **2004**, *70*, 3467−3474.
(58) Rabaey, K.; Boon, N.; Höfte, M.; Verstraete, W. Microbial phenazine production enhances electron transfer in biofuel cells. *Environ. Sci. Technol.* **2005**, *39*, 3401−3408.
(59) Liu, C. X.; Zachara, J. M.; Foster, N. S.; Strickland, J. Kinetics of reductive dissolution of hematite by bioreduced anthraquinone-2, 6-disulfonate. *Environ. Sci. Technol.* **2007**, *41*, 7730−7735.
(60) Chen, B. Y.; Hsueh, C. C.; Liu, S. Q.; Ng, I. S.; Wang, Y. M. Deciphering mediating characteristics of decolorized intermediates for reductive decolorization and bioelectricity generation. *Bioresour. Technol.* **2013**, *145*, 321−325.
(61) Martinez, C. M.; Alvarez, L. H.; Celis, L. B.; Cervantes, F. J. Humus-reducing microorganisms and their valuable contribution in environmental processes. *Appl. Microbiol. Biotechnol.* **2013**, *97*, 10293−10308.
(62) Latta, D.; Mishra, B.; Cook, R. E.; Kemner, K. M.; Boyanov, M. Stable U (IV) complexes form at high-affinity mineral surface sites. *Environ. Sci. Technol.* **2014**, *48*, 1683−1691.
(63) Pearce, C. I.; Wilkins, M. J.; Zhang, C.; Heald, S. M.; Fredrickson, J. K.; Zachara, J. M. Pore-scale characterization of biogeochemical controls on iron and uranium speciation under flow conditions. *Environ. Sci. Technol.* **2012**, *46*, 7992−8000.